

# Investigation of Some Physicochemical Properties of Camphor Sulfonic Acid (CSA)-Doped Poly(*o*-anisidine) (PoAN) and CSA-Doped PoAN/ABS Composites

R. C. PATIL, S. M. AHMED, H. SHIIGI, M. NAKAYAMA, K. OGURA

Department of Applied Chemistry, Faculty of Engineering, Yamaguchi University, Tokiwadai, Ube 755-8611, Japan

Received 29 June 1999; accepted 23 August 1999

**ABSTRACT:** Camphor sulfonic acid (CSA)-doped poly(*o*-anisidine) (PoAN) has been found to possess the electrical conductivity of 10 S/cm. This value is rather low compared to that of ( $\approx 200$  S/cm) CSA-doped polyaniline, which may arise from a limited transformation of coil-like conformation to an expanded one. Viscosity data and optical absorption spectra provided strong evidence for the existence of coil-like CSA-doped PoAN chains in *m*-cresol. The shift of IR bands of benzenoid and quinoid rings toward a lower wave number and the appearance of the bands at  $\approx 1600$  and  $1173\text{ cm}^{-1}$  (the IR is inactive but becomes active on doping) suggested the protonation of CSA-doped PoAN. The thermogravimetric profile of CSA-doped PoAN showed a five-step decomposition pattern with the thermal stability up to  $134\text{ }^\circ\text{C}$ . The mass spectra taken simultaneously with the thermogram revealed that dopant CSA is completely eliminated around  $360\text{ }^\circ\text{C}$ , but the breakdown of polymer chains does not occur very briskly at this temperature. Composites of CSA-doped PoAN with insulating acrylonitrile-butadiene-styrene copolymer (ABS) were fabricated, and it was found that the composites showed a percolation behavior in which the electrical conductivity rose sharply at about 4 weight % of CSA-doped PoAN in the ABS composite. The STM data demonstrated the formation of a continuous path at the percolation threshold. The Poole-Frenkel effect was observed for the conduction scheme in the CSA-doped PoAN/ABS composite. © 1999 John Wiley & Sons, Inc. *J Polym Sci A: Polym Chem* 37: 4596–4604, 1999

**Keywords:** poly(*o*-anisidine); composite; percolation threshold; conductivity; molecular conformation

## INTRODUCTION

The great potentiality of conducting polymers, especially polyaniline, toward practical applications has attracted tremendous attention, and this polymer has been studied in more and more detail for the last decade. The usefulness of polyaniline in variety of applications includes printed circuit boards,<sup>1</sup> electrochromic displays,<sup>2</sup> antistatic coatings,<sup>3</sup> corrosion inhibitors,<sup>1,4</sup> electromagnetic shielding material,<sup>1,5</sup> and so on. Sometimes it is

desirable to obtain polyaniline that is soluble and processable rather than highly conductive. The processability and solubility in different solvents have been achieved by using large-size dopant molecules such as camphor sulfonic acid, dodecyl benzene sulfonic acid, methane sulfonic acid, and so forth. Several reports are available in the literature<sup>6–8</sup> on the protonation of polyaniline by these acids. However, analogues of polyaniline, such as poly(*o*-toluidine) and poly(*o*-anisidine), have not been studied in detail despite their usefulness in some applications such as antistatic coatings for which very high conductivity is not essential.

In the present work, the camphor sulfonic acid-doped poly(*o*-anisidine) was prepared and charac-

Correspondence to: K. Ogura

*Journal of Polymer Science: Part A: Polymer Chemistry*, Vol. 37, 4596–4604 (1999)  
© 1999 John Wiley & Sons, Inc. CCC 0887-624X/99/244596-09

terized with various techniques. Furthermore, percolation behavior was found for the composite of CSA-doped PoAN with ABS, and the conduction scheme of this composite was discussed.

## EXPERIMENTAL

All chemicals used were of analytical reagent grade. Poly(*o*-anisidine) doped with HCl was synthesized following the previously described procedure.<sup>9</sup> The HCl-doped PoAN was then converted to the base form by treating it with 3% aqueous (NH<sub>4</sub>)OH solution, followed by washing with distilled water, methanol, and diethyl ether. To obtain CSA-doped PoAN, the emeraldine base of PoAN [EB(PoAN)] was mixed with *d, l* camphor sulfonic acid in the molar ratio of 1 : 2 for EB (PoAN) (tetramer) to CSA by pestling with an agate mortar in an inert atmosphere. The CSA-doped PoAN/ABS composites were prepared by the following procedure. The 8 wt % solution of CSA-doped PoAN in *m*-cresol was first made by using ultrasonics for 1 h at 50 °C, and the appropriate amount of the resulting viscous deep green solution was then mixed with 10 wt % solution of ABS matrix polymer at room temperature.

The conductivities of CSA-doped PoAN and its composite with ABS were measured by the two-probe method using a Hokuto Denko galvanostat (model HA-501). The samples for this measurement were made by casting CSA-doped PoAN solutions with and without ABS on a comb-shaped Pt microelectrode and removing the solvent. UV-visible absorption spectra of *m*-cresol solutions of CSA-doped PoAN were recorded on a Shimadzu double beam spectrophotometer (Model 2200). Thermogravimetric/mass analyses were performed on a Jeol MS-TG/DTA (Model 220) under He atmosphere. About 11.41 mg of CSA-doped PoAN was placed in a sample holder, and the temperature was changed from 40 to 900 °C at the programmed heating rate of 5 °C/min. Mass spectra were recorded simultaneously during thermal analysis. The volatile material arising from the polymer sample as a function of temperature was fed into the bench-top quadrupole mass spectrometer and the mass spectra were continuously monitored through the computer-controlled system. After recording the total ion chromatogram from 40 to 900 °C, the mass spectra were deduced at selective temperature ranges as mentioned in the text. Fourier transform infrared spectroscopic measurements of EB and CSA-doped PoAN in

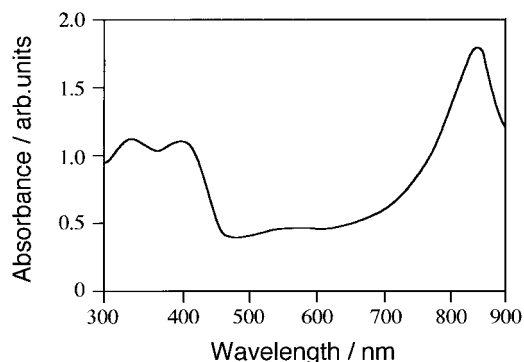


**Figure 1.** UV-visible absorption spectrum of CSA-doped PoAN in *m*-cresol.

KBr pellets were carried out using a Shimadzu FTIR (Type 8100 M) spectrometer. The viscosity data of CSA-doped PoAN solution in *m*-cresol were obtained with an Ostwald type viscometer (Sibata, No. 3) at 25 ± 1 °C. Scanning tunneling microscopic images were taken using a Nanoscope II instrument from Digital Instruments. Samples were prepared by casting the CSA-doped PoAN/ABS solution on a steel plate and evaporating the solvent at 50 °C. The measurements were performed on a constant current mode with a bias voltage of 30 mV and a tunneling current of 2.0 nA. Before taking micrographs, the alignment of the tip with the sample was ensured. All images exhibited in the text are real-time photographs taken directly from the computer screen.

## RESULTS AND DISCUSSION

Figure 1 represents optical absorption spectra of CSA-doped PoAN. The peak at ≈860 nm indicates the formation of emeraldine salt, while those at ≈340 nm and 440 nm correspond to  $\pi$ - $\pi^*$  transition and polaron band, respectively.<sup>10</sup> The broadening in the region around 560 nm suggests the formation of a pernigraniline phase during the polymerization. Although the conversion of the emeraldine base to a salt form, as evidenced by the peak at ≈860 nm, demonstrates that PoAN was effectively protonated, the conductivity of CSA-doped PoAN was found to be 10 S/cm. This value is 20× lower than that reported for CSA-doped polyaniline. The lower conductivity of CSA-doped PoAN can be explained with the help of the respective contributions of the intermolecular and intramolecular components in controlling overall conductivity. The intermolecular compo-

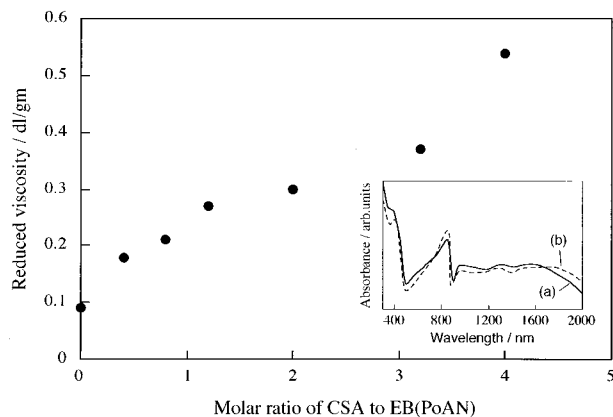


**Figure 2.** Reduced viscosity of CSA-doped PoAN solutions in *m*-cresol as a function of the molar ratio of CSA to EB (PoAN). Inset represents the absorption spectra of CSA-doped poly(*o*-anisidine) at two different molar ratios of CSA to EB (PoAN) in *m*-cresol solution: (a) 4 and (b) 2. The concentration of EB(PoAN) was always 0.015%.

ment is related to the polymer conformation. It was previously proposed by MacDiarmid et al.<sup>11</sup> that the change in conformation from coil like to expanded coil tends to decrease conjugation defects that facilitate the delocalization of electrons through a polymer chain very effectively. The change in such conformation can be evaluated by measuring reduced viscosity. The expansion of coil should result in a rise in hydrodynamic volume of the polymer, leading to an increase of reduced viscosity.

In Figure 2 the reduced viscosity is plotted against the molar ratio of CSA to EB(PoAN). It is obvious that there's hardly any expansion of coil, which is the result of very little increase in the hydrodynamic volume. The optical absorption spectra provides additional support for this view. In the inset of Figure 2, the typical spectra for the solutions containing EB (PoAN) and CSA at the molar ratio of 1 : 2 [Fig. 2(a)] and 1 : 4 [Fig. 2(b)] are shown to be in the range of 300 to 2000 nm. The absence of free carrier tail at  $\approx 1000$  nm, which is considered a measure of the extent of transformation, clearly reveals the polymer chains are still in a coil-like conformation. This strongly suggests that the intramolecular component of polymer (i.e., delocalization of electrons) is not very effective, which may cause relatively low conductivity as compared to that of CSA-doped PANI.

On the other hand, the intermolecular component is mainly related to polymer chain packing.

It is well known that the presence of a bulky methyl group tends to enhance a disorder in the polymer backbone as well as to cause a large increase in the interlayer separation.<sup>12</sup> The methoxy group being bulkier than methyl should cause a poor packing of the chains, allowing a weak interchain charge transfer in CSA-doped PoAN. Moreover, the opening of the coil-like conformation, which tends to promote the linear conformation necessary for crystallization, is inhibited, and this in turn limits the intensity of the intermolecular component. Limited effectiveness of the intermolecular as well as the intramolecular components therefore leads to restricted enhancement of the conductivity for CSA-doped PoAN.

Nevertheless, it is important to know why coil-like chains of CSA-doped PoAN cannot be expanded in *m*-cresol. This is probably related to the steric hindrance of the methoxy group of PoAN influencing an interaction between phenyl rings of PoAN and *m*-cresol. The position of the methoxy group at the ortho position of the aniline ring may prevent the phenyl rings of PoAN from interacting with *m*-cresol and stacking. As a result, the interaction between the polymer chain and the solvent may be limited to a small extent, leading to a little solvation of the positive charges on the polymer chain and of the negative CSA<sup>-</sup> ions.<sup>11</sup> This may lead to a weak electrostatic repulsion between positively charged units of the polymer, blocking the transformation to the expanded coil conformation.

The IR spectra of the undoped and doped emeraldine bases of PoAN are shown in Figure 3. The key bands for unprotonated EB occur at 3350, 2947, 1588, 1500, 1452, 1407, 1320, 1254, 1209, 1169, 1116, and 1028  $\text{cm}^{-1}$  [Fig. (3b)]. The peaks appearing at 3350 and 2947  $\text{cm}^{-1}$  are assigned to the N—H stretching vibration of the  $\text{C}_6\text{H}_4\text{—NH—C}_6\text{H}_4$  group and to the C—H stretching vibration of the  $\text{OCH}_3$  group belonging to aniline, respectively. The bands at 1588 and 1500  $\text{cm}^{-1}$  are due to the quinoid and benzenoid rings, respectively. The bands observed at 1407 and 1452  $\text{cm}^{-1}$  can be attributed to the C—H bending mode of the benzene ring and the  $\text{OCH}_3$  group, respectively. The two bands at 1320 and 1254  $\text{cm}^{-1}$  are characteristic of the vibrational absorption assignable to the C—N stretching modes of aromatic amine of the emeraldine base.<sup>13</sup> The band at 1209  $\text{cm}^{-1}$  corresponds to the C—H stretching of the 1-2-4 substituted benzene ring, confirming that polymer chains are formed through head-to-

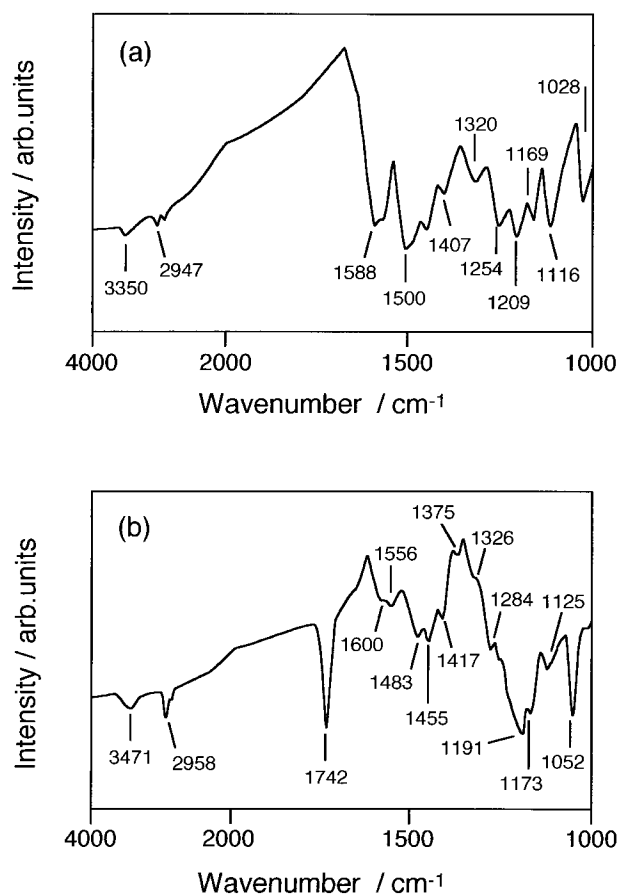


**Figure 3.** IR spectra of: (a) EB (PoAN) and (b) CSA-doped PoAN.

tail coupling.<sup>14</sup> The peaks at 1169 and 1116  $\text{cm}^{-1}$  are due to the C—H in plane bending, and the peak at 1169  $\text{cm}^{-1}$  can be ascribed to the C—C—N or the N—H bending.<sup>15</sup> Finally, the peak at 1028  $\text{cm}^{-1}$  is related to the C—O—C stretching from the  $\text{CH}_3\text{—O—PhNH}_2$  group.<sup>14</sup>

The IR spectrum of CSA-doped PoAN exhibits some interesting features in comparison with that of EB [Fig. 3(b)]. The band at 3471  $\text{cm}^{-1}$  due to the OH stretching vibration probably arises from adsorbed water. Because of the appearance of this peak, the contribution from the N—H stretching vibration was completely masked. The peak at 2958  $\text{cm}^{-1}$  due to the C—H vibration becomes more distinct because of the additional contribution from  $\text{CH}_3$  and  $\text{CH}_2$  groups belonging to CSA. Furthermore, a definite peak at 1742  $\text{cm}^{-1}$  assignable to the C=O stretching vibration reveals that CSA is incorporated in the polymer backbone. A red shift of the peaks due to quinoid and benzenoid vibrations from 1588 to 1556 and from 1500 to 1483  $\text{cm}^{-1}$ , respectively, indicates the

transformation of emeraldine base to the semiquinoid form (polaron), thereby confirming the protonation of the emeraldine base.<sup>16</sup> The appearance of the absorption bands at 1600 and at 1173  $\text{cm}^{-1}$  are assignable to the C—C ring stretching mode and the C—H bending or ring amine bending vibration, respectively.<sup>15</sup> Theoretical studies of Raman spectra demonstrate that these modes are attributed to  $\text{A}_g$  and  $\text{B}_{3g}$  Raman active vibrations.<sup>17,18</sup> These bands are normally infrared inactive but become active if polarons are induced by some protonation process. Hence, the appearance of these bands for the CSA-doped PoAN gives an evidence for the protonation of the polymer. An additional band at 1284  $\text{cm}^{-1}$ , which was masked by the sharp band at 1254  $\text{cm}^{-1}$  for the undoped EB, is ascribed to the mixed mode of the C—H bending and the C—N stretching.<sup>19</sup> The band at 1125  $\text{cm}^{-1}$  originates from the C—( $\text{CH}_3$ )<sub>2</sub> skeletal vibration of CSA<sup>-</sup> ions, while that at 1052  $\text{cm}^{-1}$  is related to the symmetric and anti-symmetric stretching modes of the  $\text{SO}_3^-$  group.<sup>14</sup>

The thermal behavior of CSA-doped PoAN is depicted along with the DTG curve in Figure 4. The DTG curve clearly defines a five-step decomposition pattern. The details about the weight loss and the fragments generated in the decomposition at each step are shown in Table I. The weight loss in the first step ( $\approx 1.4\%$ ) is attributed to the desorption of superficial water molecules associated with the doped PoAN. The mass spectra presented in Figure 5(a) reveals an intense fragment of water molecules (stage I). The CSA-doped PoAN then remains stable up to 134 °C. The second step, extending up to 265 °C with weight loss of 13.4%, indicates the loss of sulfinyl

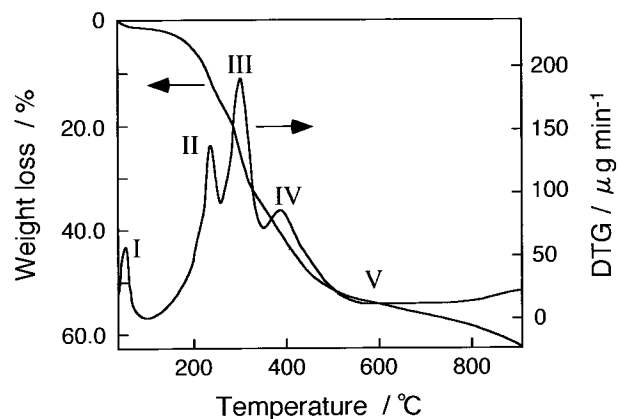


**Figure 4.** Thermal pattern of CSA-doped PoAN taken at the programmed heating scan rate of 5 °C/min.

**Table I.** Details about the Decomposition Pattern of CSA-Doped PoAN

Step	Temperature Range/°C	Weight Loss/%	Fragments Obtained
I	40–134	1.4	18 : H <sub>2</sub> O
II	134–265	13.4	18 : H <sub>2</sub> O 32 : O <sub>2</sub> 48 : SO <sup>+</sup> 64 : SO <sub>2</sub> <sup>+</sup> } CSA <sup>-</sup> 135 : CSA <sup>-</sup> without CH <sub>2</sub> SO <sub>3</sub> <sup>-</sup> 150 : CSA <sup>-</sup> without SO <sub>3</sub> <sup>-</sup>
III	265–356	21.0	32 : O <sub>2</sub> 48 : SO <sup>+</sup> 64 : SO <sub>2</sub> <sup>+</sup> 79 : SO <sub>3</sub> <sup>+</sup> 93 : CH <sub>2</sub> SO <sub>3</sub> <sup>-</sup> } CSA <sup>-</sup> 107 : C <sub>6</sub> H <sub>4</sub> OCH <sub>3</sub> 121 : C <sub>6</sub> H <sub>4</sub> OCH <sub>3</sub> NH <sup>+</sup> } from polymer backbone
IV	356–533	17.2	151 : CSA <sup>-</sup> without SO <sub>3</sub> <sup>-</sup> Some fragments from CSA <sup>-</sup> as mentioned above together with those from polymer degradation
V	533–900	10.0	28 : N <sub>2</sub> 44 : CO <sub>2</sub>

(SO<sup>+</sup>, m/z 48), sulfonyl (SO<sub>2</sub><sup>+</sup>, m/z 64) along with CSA<sup>-</sup> anions without CH<sub>2</sub>SO<sub>3</sub><sup>-</sup> (m/z 135) and SO<sub>3</sub><sup>-</sup> (m/z 150) group (stage II) [Fig. 5(b), Table I]. The observation that only dopant CSA undergoes decomposition in this temperature range [Fig. 5(b)] also suggests that no chain degradation occurs. The appearance of a fragment of m/z 18 arises from the strongly bound water molecules associated with the dopant CSA; this supports the results reported earlier by Boyle et al.<sup>20</sup> Further elevation of the temperature, up to 356 °C, demonstrates that several fragments are due to dopant CSA<sup>-</sup> together with some fragments from the polymer backbone, especially at m/z 107 and 121 (stage III) [Fig. 5(c), Table I]. Although the fragments with m/z 165 and 180 are not exactly assignable, their origin is probably from the polymer backbone. At temperatures higher than 356 °C (stage IV), the polymer chain degradation is initiated, and various fragments from the polymer backbone (m/z 149, 180, 210, 241, 255, and 269) are clearly visible in the mass spectra. The existence of fragments from CSA, particularly those of the oxygen, sulfinyl, and sulfonyl groups in the fourth stage of decomposition [Fig. 5(d)], might be attributed to the sulfonation of the polymer chain. It was previously proven by Boyle et al.<sup>20</sup> for PANI–H<sub>2</sub>SO<sub>4</sub> system that the degrada-

tion mechanism proceeds with chain sulfonation accompanied by chain oxidation. It is likely that a similar kind of reaction occurs, in which the sulfonated polymer backbone undergoes degradation, releasing fragments of the oxygen, sulfinyl, and sulfonyl groups along with various fragments from the polymer chain. With further heating of the sample beyond 800 °C, only a loss of CO<sub>2</sub> is observed (stage V) [Fig. 5(e)], and the total weight loss for all steps was found to be ≈63%.

A plot of conductivity versus weight % of CSA-doped PoAN in ABS (Fig. 6) indicates that the conductivity of the composite increases with increasing weight % of CSA-doped PoAN, and a sharp increase in conductivity appears at about 4% of conducting particles. This value is the percolation threshold, and the occurrence of the percolation may be related to the finite and infinite clusters that are formed by the Brownian movement of molecules toward each other and their aggregation. At 20% concentration of PoAN–CSA in the composite, the population of conducting particles is relatively high compared to that at the threshold value (4%). These particles may come in contact with each other (interparticulate contacts) to form infinite clusters. Electrons can travel through these clusters very easily, and this situation leads to the enhancement of electrical

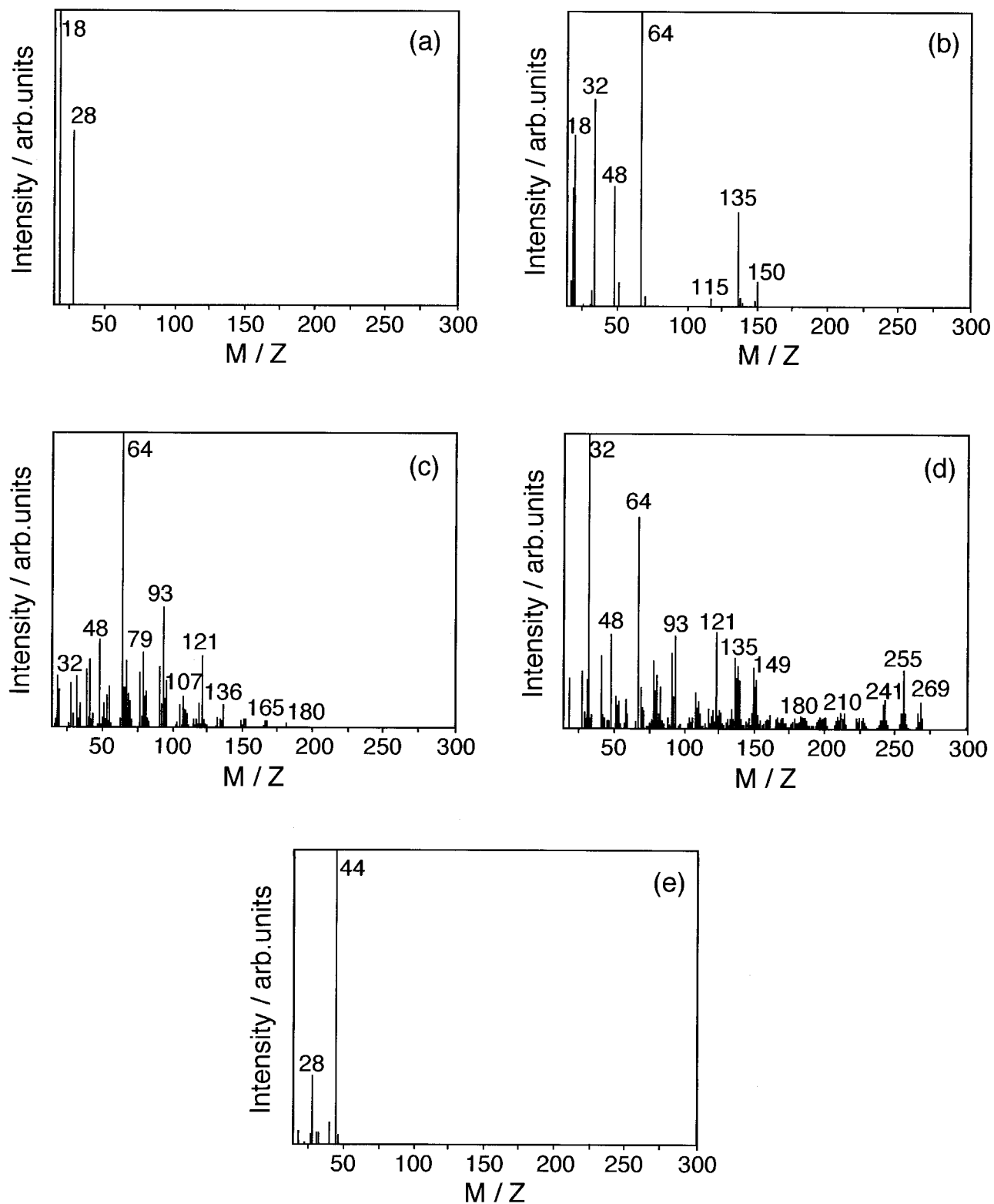


**Figure 5.** Mass spectra of CSA-doped poly(*o*-anisidine) taken at: (a) 80 (b) 220 (c) 300 (d) 380 and (e) 890 °C.

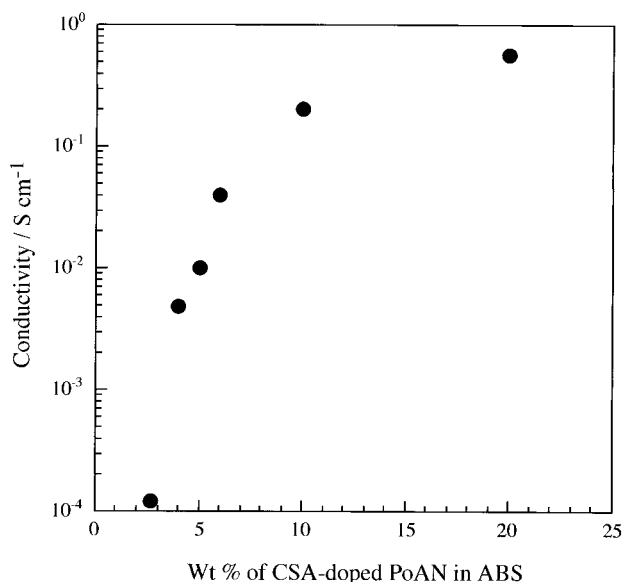


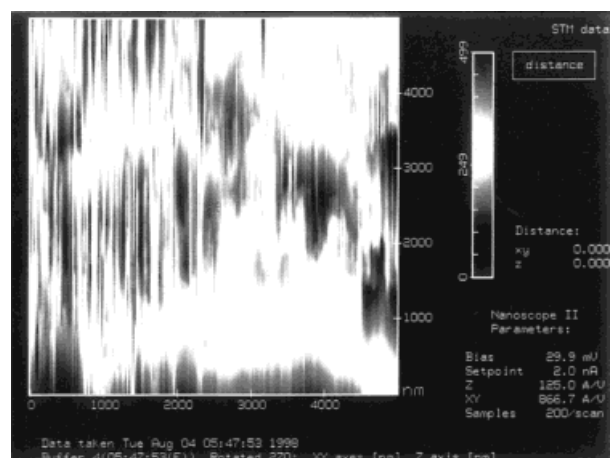
**Figure 6.** Plot of electrical conductivity of CSA-doped PoAN/ABS polyblends as a function of the weight percentage of CSA-doped PoAN.

conductivity. However, as the number of conducting particles in the composite is reduced, the available number of particles tends to form a self-assembling network. The charge transport is permitted through such a least-resistive path, which is especially true at the percolation value. Below the threshold value, however, the interdomains (conducting particles) are isolated, and as a result, finite clusters become a controlling factor in determining the conductivity. As the interdomain distance increases, the electron hopping through the finite clusters becomes more difficult, resulting in the drop in conductivity.

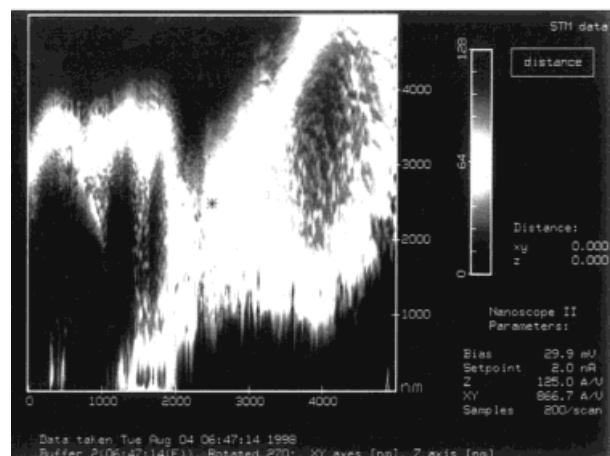
The STM analysis was carried out in order to prove that the observed conductivity at the percolation threshold was the result of the formation of a continuous path of conducting particles. Figure 7(a) represents an STM image of CSA-doped PoAN alone, in which the bright regions are quite evident. In Figure 7(b), the STM micrograph of the composite containing 20% of CSA-doped PoAN particles in ABS is shown, in which the brighter region indicates a PoAN-rich phase, while the darker is that of ABS.<sup>21</sup> A very close contact between CSA-doped PoAN particles is evidently seen. For the composite with the percolation threshold, however, the aggregation is observed to form a continuous path, indicating the formation of an interconnecting network [Fig.

8(a)]. Interestingly, the STM image of the composite with CSA-doped PoAN below the concentration at the percolation threshold still shows some interparticle contacts, but at the same time the decrease in the particle size, as well as some isolated particles [Fig. 8(b)], is apparent.

The STM results reveal that the binodal type of phase separation exists in the composites in which interconnected regions of ABS-rich and CSA-doped PoAN-rich phases are formed.<sup>22</sup> It is interesting to know the effect of such phase-segregated morphology on the electrical properties of these conducting polymers, which can be well understood with the help of current-voltage characteristics [Fig. 9(a,b)]. Figure 9(a) shows some non-linear relationship between current and voltage, especially at a higher voltage region, for the CSA-doped PoAN/ABS composites with different com-

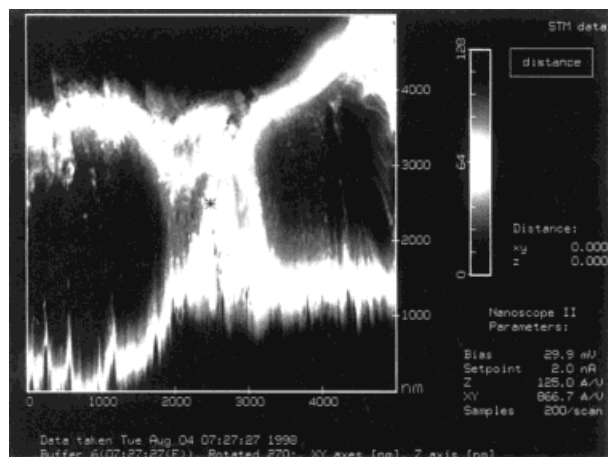


(a)

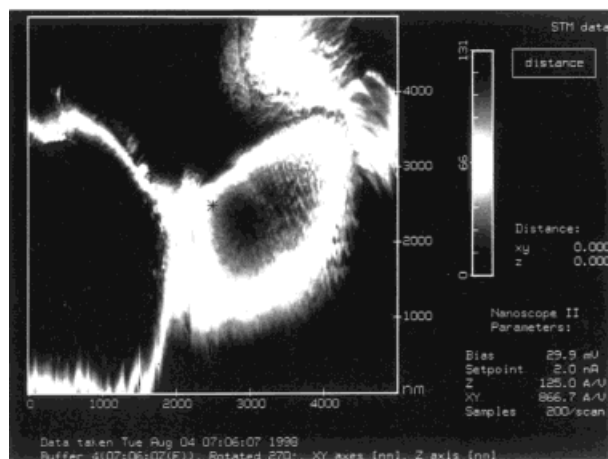


(b)

**Figure 7.** STM images of (a) CSA-doped PoAN and (b) CSA-doped PoAN (20 wt %)/ABS (80 wt %).



(a)



(b)

**Figure 8.** STM images of CSA-doped PoAN/ABS polyblends with different weight fractions of CSA-doped PoAN: (a) 4% and (b) 2.66%.

positions. The observed nonlinearity may arise from nonohmic charge transport, processes such as Schottky emission (SE), Poole–Frenkel effect (PF), and space charge limited conduction (SCLC),<sup>23</sup> in which the composite system is essentially considered as a series of junctions formed by conducting–insulating–conducting elements. As a Pt microelectrode was used here as the substrate for our experiments, the possibility of Schottky effect may be ruled out, because Pt has a high work function and forms ohmic contact with p-type material such as PoAN.<sup>24</sup> The SCLC mechanism is also not valid because a plot of I-V characteristics on log–log scale did not yield the slope  $n > 2$ , as expected for SCLC; rather, it gave the value of  $\approx 1.2$ . Therefore, the Poole–Frenkel

effect was examined. The current for semiconducting materials in the presence of impurity centers is given by eqs. (1), (2), and (3):

$$I = I_0 \exp(\beta_{PF} F^{1/2} / 2kT) \quad (1)$$

$$I_0 = e\mu(N_d/N_t)^{1/2} F \exp[-(E_d + E_t)/2kT] \quad (2)$$

$$\beta_{PF} = (e^3/4\pi\epsilon K)^{1/2} \text{ and } F = V/d \quad (3)$$

where  $F$  is electric field ( $= V/d$ );  $V$ , applied voltage; and  $d$ , the thickness (here the interdomain distance).  $\beta_{PF}$  is Poole–Frenkel constant;  $e$ , electronic charge;  $\mu$ , the carrier mobility;  $N_d$ , the density of donor states;  $N_t$ , the density of trapping states; and  $E_d$  and  $E_t$  the energy levels for donor and trapping centers below the conduction band, respectively.

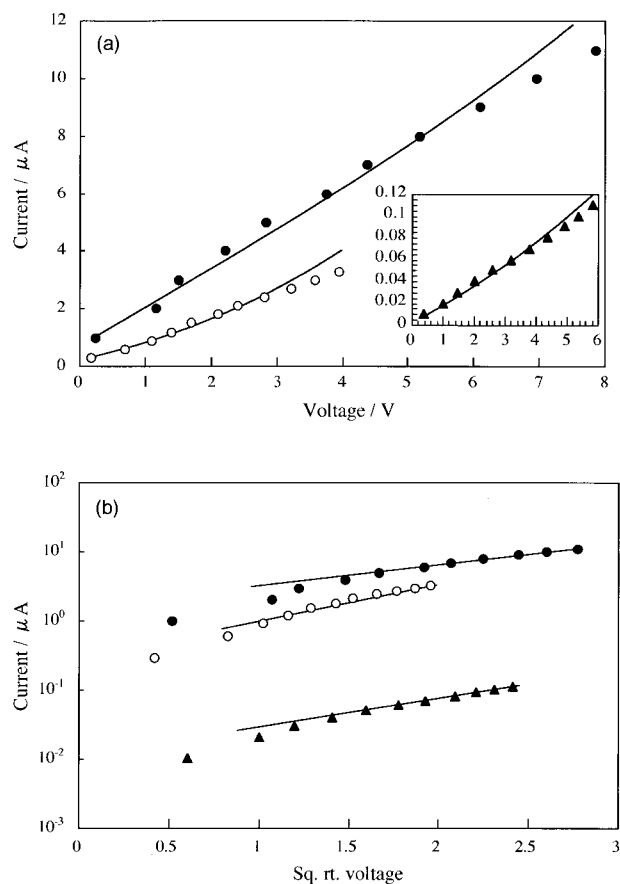


**Figure 9.** (a) I-V characteristics of CSA-doped PoAN/ABS polyblends on a linear scale depicting nonohmic behavior. The concentrations of CSA-doped PoAN were: 20% (●), 10% (○), and 4% (▲). (b) Poole–Frenkel plots of the I-V characteristics that were drawn based on the result of (a).

The Poole–Frenkel parameter is mainly related to dielectric constant ( $\epsilon$ ) of the material. From the above equations it can be seen that at a constant temperature, the plot of  $\log I$  versus  $V^{1/2}$  should be linear. In fact, the logarithmic  $I$  is linearly related to the square root of voltage, as depicted in Figure 9(b), suggesting that the Poole–Frenkel effect is quite operative for CSA-doped PoAN/ABS composites. The minor deviations at low applied voltages may be due to the transition from linear to nonlinear behavior, since the Poole–Frenkel effect is predominant in the high field region. Thus, from above discussion it may be understood that the slope of Poole–Frenkel plots would be dependent not only on the  $\beta_{PF}$  but also on the interdomain distance,  $d$ . Therefore, these two parameters are both related to the values of the dielectric constant and of the separation between conducting domains, which are very dependent on the concentration of ABS in the blend.

## CONCLUSIONS

The electrical conductivity of poly(*o*-anisidine), one of the substituted polyanilines, was enhanced to 10 S/cm by doping with camphor sulfonic acid. The PoAN chains were found to adopt coil-like conformation, which limits its conductivity to 10 S/cm compared to polyaniline ( $\approx 200$ – $400$  S/cm). The thermal analysis provided important information about the polymer degradation and showed that dedoping of the polymer started at  $\approx 134$  °C, and the process continued slowly up to 360 °C. The composites of CSA-doped PoAN with ABS were fabricated, and the percolation behavior (4 weight %) was observed. The formation of the conducting path at the percolation threshold was proved by the STM observation, and it was demonstrated that the conduction follows the Poole–Frenkel mechanism.

One of the authors (RCP) is thankful to Venture Business Laboratory for providing PDF.

## REFERENCES AND NOTES

- Wessling, B. *Synth Met* 1998, 93, 143.
- Hugot-Le Goff, A. In *Handbook of Organic Conductive Molecules and Polymers*; Nalwa, H. S., Ed.; Wiley-Interscience: New York, 1997; Volume 3, pp. 745–782.
- Olcani, A.; Abe, M.; Ezoe, M.; Doi, T.; Miyata, T.; Miyake, A. *Synth Met* 1993, 57, 3696.
- McAndrew, T. P. *Trip* 1997, 5(1), 7.
- Epstein, A. J.; Yue, J. U.S. Patent 5137991, 1992.
- Cao, Y.; Smith, P.; Heeger, A. J. U.S. Patent 5232631, 1993.
- Cao, Y.; Smith, P.; Heeger, A. J. *Synth Met* 1993, 3(514), 55–57.
- MacDiarmid, A. G.; Epstein, A. J. *Synth Met* 1994, 65, 103.
- Cao, Y.; Smith, P.; Heeger, A. J. *Synth Met* 1989, 32, 263.
- Chen, S. A.; Hwang, G. W. *J Am Chem Soc* 1995, 117, 10055.
- Avlyanov, J. K.; Min, Y.; MacDiarmid, A. G.; Epstein, A. J. *Synth Met* 1995, 72, 65.
- Pouget, J. P.; Hsu, C. H.; MacDiarmid, A. G.; Epstein, A. J. *Synth Met* 1995, 69, 119.
- Ping, Z. *J Chem Soc, Faraday Trans* 1996, 92(17), 3063.
- Bellamy, L. J. In *The Infrared Spectra of Complex Molecules*; Chapman & Hall: London, 1975; pp. 75, 131, 408.
- Ping, Z.; Nauer, G. E.; Neugebauer, H.; Theiner, J. *J Electroanal Chem* 1997, 420, 301.
- Harada, I.; Furukawa, Y.; Ueda, F. *Synth Met* 1989, 29, E-303.
- Quillard, S.; Louarn, G.; Buisson, J. P.; Lefrant, S.; Masters, J.; MacDiarmid, A. G. *Synth Met* 1992, 525, 49–50.
- Kostic, R.; Rakovic, D.; Davidova, I. E.; Gribov, L. A. *Phys Rev B*, 1992, 45, 728.
- Furukawa, Y.; Ueda, F.; Hyodo, Y.; Harada, I.; Nakajima, T.; Kawagoe, T. *Macromolecules* 1988, 21, 1297.
- Boyle, A.; Penneau, J. F.; Genies, E.; Riekel, C. *J Poly Sci: Part B Poly Phys* 1992, 30, 265.
- Chen, S. A.; Hwang, G. W. *Polymer* 1997, 38(13), 3333.
- Yang, C. Y.; Cao, Y.; Smith, P.; Heeger, A. J. *Synth Met* 1993, 53, 293.
- Simmons, J. G.; Maissel, L. I.; Glang, R. In *Handbook of Thin Film Technology*; McGraw-Hill: New York, 1976, Chapter 14.
- Radhakrishnan, S.; Khedkar, S. P. *Synth Met* 1996, 79, 219.